Available online at www.sciencedirect.com

ScienceDirect

journal homepage: www.elsevier.com/locate/he

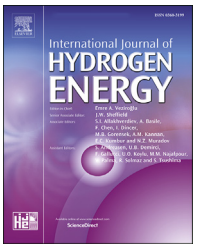

Oxidative steam reforming of acetic acid on Ni catalysts: Influence of the La promotion on mesostructured supports

Pedro J. Megía, Anabel Morales, Arturo J. Vizcaíno, José A. Calles, Alicia Carrero *

Chemical and Environmental Engineering Group, Rey Juan Carlos University, c/Tulipán s/n, Móstoles 28933, Spain

HIGHLIGHTS

- SBA-15 and mesoporous CeO_2 were used as supports for reforming Ni catalysts.
- Mesoporous CeO_2 improved the catalytic performance of Ni and reduced coke deposited.
- La_2O_3 promotion prevented Ni sintering getting better Ni dispersion.
- Ni supported over La_2O_3-mesoporous CeO_2 showed the best catalytic performance.

ARTICLE INFO

Article history:
Received 30 November 2022
Received in revised form
8 May 2023
Accepted 25 June 2023
Available online xxx

Keywords:
Renewable hydrogen
Mesoporous ceria
Lanthanum
SBA-15
Nanocasting
Bio-oil

ABSTRACT

In this work, the support effect and the La_2O_3 promotion of Ni-based catalysts on the oxidative steam reforming of acetic acid as bio-oil model compound has been studied. Ni/SBA-15 showed the worst catalytic performance with an acetic acid conversion dropping below 30% at 500 °C ascribed to active phase oxidation. In contrast, Ni supported over mesoporous CeO_2 (CeO_2-m) reached better catalytic performance and lower coke formation due to the higher Ni dispersion and oxygen mobility of the support. On the other hand, La_2O_3 promotion to SBA-15 and CeO_2-m led to even higher Ni dispersion and prevented sintering during the reforming reaction. This effect resulted in an improvement in the catalytic performance for both promoted samples. As a consequence of low Ni crystallite size and high oxygen mobility, Ni/La_2O_3–CeO_2-m reached almost complete conversion (~96%), the highest hydrogen yield (~53%) maintained for 5 h with the lowest coke formation (62.3 $mg_{coke} \cdot g_{cat}^{-1} \cdot h^{-1}$).

Introduction

Hydrogen is increasingly getting much more attention as an energy carrier, particularly when it is produced from renewable feedstock such as biomass. It is well established that biomass-to-energy processes allow a neutral carbon emission scenario. Biomass reduces global warming emissions since it absorbs CO_2 from the natural environment during photosynthesis [1–3]. As biomass can store energy through chemical bonds between carbon, hydrogen, and oxygen, through thermochemical processes, such as pyrolysis or hydrothermal

* *Corresponding author.*
E-mail address: alicia.carrero@urjc.es (A. Carrero).

https://doi.org/10.1016/j.ijhydene.2023.06.283

liquefaction, it is possible to break down these bonds to release vast amounts of energy to produce bio-oil [4–6]. However, bio-oil is considered a poor quality fuel due to the presence of oxygenated hydrocarbon compounds in its composition. Bio-oil can be revalorized by a catalytic reforming process producing renewable hydrogen. In this regard, in recent years, many research groups have paid attention to catalytic steam reforming of bio-oil [7–9]. Steam reforming, being an endothermic reaction, has high energy requirements that constrain its implementation at an industrial scale. This drawback can be addressed by co-feeding oxygen or air along with the steam, resulting in oxidative steam reforming. The presence of oxygen will reduce the energy requirements and the proportion of CO which would be oxidized to CO_2 [10]. The overall equation that describes this process can be represented as:

$$C_nH_mO_k + pO_2 + (2n - k - 2p)H_2O \rightarrow nCO_2 + \left(2n + \frac{m}{2} - k - 2p\right)H_2 \quad (1)$$

One of the main challenges in the oxidative steam reforming process is maintaining the catalyst's stability in the presence of oxygen. Nickel has been deeply studied as an active phase for reforming purposes given its high activity toward C–C bond breaking and low price. However, the formation of carbon deposits and sintering is the major drawback of their applications [11]. Not with understanding that coke deposition is lower in oxidative steam reforming compared to traditional steam reforming, hot spots due to exothermicity of the oxidation reactions can lead to sintering gradually reducing the catalyst activity [12]. Moreover, an oxidizing atmosphere may cause active phase oxidation resulting in less active species, the reason why oxygen feeding should be controlled [13,14]. The nature of the support has also been reported as a crucial role in catalyst properties including the deactivation behavior [15]. To enhance the catalytic performance of nickel-based catalysts, it is important to use mesoporous structures with a high surface area which may allow higher metal dispersion [16]. In this regard, SBA-15 as support has been widely studied for reforming purposes given its ordered hexagonal mesostructure [17–19]. On the other hand, ceria-containing supports have been reported to have a proper interaction with nickel particles also hindering carbon formation. This is ascribed to the ability of CeO_2 to promote coke gasification apart from being active in the water-gas shift reaction due to its capacity to store, release, and transport oxygen as reported elsewhere [20]. The main problem of using ceria as a support is its non-porous structure with low surface area [21]. However, it can be faced by preparing mesoporous ceria, thus taking advantage of oxygen mobility but allowing high dispersion [22]. Despite this, the use of ceria-based mesoporous structures is rarely reported for reforming purposes. Apart from that, the catalytic performance could be further improved by including promoters in the catalyst formulation [23–25]. In a previous work [26], it was verified how La_2O_3 promotion to Co/SBA-15 in glycerol steam reforming, prevented metal sintering along with a decrease in coke deposition ascribed to the formation of $La_2O_2CO_3$ which can react with carbon deposits releasing CO and regenerating La_2O_3. Similarly, Charisiou et al. [27] reported higher dispersion of Ni^0 species in La_2O_3-promoted Ni/Al_2O_3 catalysts, allowing higher glycerol conversion towards gaseous products. Guo et al. [28], achieved lower Ni particle size with the promotion of lanthanum to Ni/SiO_2, resulting in a better catalytic performance in acetic acid steam reforming. They observed that the presence of La_2O_3 in the catalyst formulation greatly decreased the coke deposition apart from inhibiting the generation of encapsulating coke. Nonetheless, the research about the use of mesostructured supports for acetic acid oxidative steam reforming is limited. Based on this background, the effect of lanthanum addition to a series of Ni catalysts supported over SBA-15 and mesostructured ceria synthesized by nanocasting is studied in the oxidative steam reforming of acetic acid as a model compound of bio-oil aqueous phase.

Methodology

Catalysts preparation and characterization

To study the effect of lanthanum addition on nickel-based catalysts, two supports synthesized in the lab were used: a mesostructured SBA-15 and mesoporous ceria using SBA-15 as a hard template. The SBA-15 material was prepared following a hydrothermal method as described elsewhere [29]. As stated before, SBA-15, apart from being used as a support, was used as hard-templated to synthesize the mesoporous ceria (CeO_2-m) which was prepared by nanocasting [30] using $Ce(NO_3)_3 \cdot 6H_2O$ as the metal precursor. All the supports were subsequently modified by lanthanum incorporation using aqueous solutions of $La(NO_3)_3 \cdot 6H_2O$ to reach a La loading of about 10 wt% in the support. The incipient wetness impregnation method was used for SBA-15 while the wet impregnation technique was selected for the mesoporous CeO_2 given its lower surface area and pore volume. After that, samples were calcined at 550 °C for 5 h to completely remove the lanthanum precursor. Finally, Ni incorporation was performed following the same impregnation procedure described for La, using an aqueous solution of $Ni(NO_3)_2 \cdot 6H_2O$ to get Ni loadings around 7 wt % in the calcined catalysts. The samples were subsequently calcined at 550 °C for 5 h.

Synthesized materials were characterized using different techniques. ICP-AES was used to determine the Ni and La contents in the materials in a Varian Vista-PRO AX CCD-Simultaneous ICP-AES spectrophotometer. SBA-15-based samples were previously dissolved by acidic digestion using H_2SO_4 and HF while HNO_3 and H_2O_2 were used to dissolve ceria-based samples. Textural properties were determined on a Micromeritics TRISTAR 3000 sorptometer measuring nitrogen adsorption-desorption isotherms at 77K. Before the adsorption, samples were outgassed under vacuum at 200 °C for 4 h. Surface areas were estimated according to the Brunauer-Emmett-Teller method (BET). XRD diffractograms were acquired on a Philips X'PERT PRO diffractometer using Cu Kα radiation. To determine the crystalline phases, the obtained patterns were compared to those from the JCPDS index. The mean crystallite diameter was calculated by applying the

Please cite this article as: Megía PJ et al., Oxidative steam reforming of acetic acid on Ni catalysts: Influence of the La promotion on mesostructured supports, International Journal of Hydrogen Energy, https://doi.org/10.1016/j.ijhydene.2023.06.283

Scherrer equation in the main diffraction line of Ni. The catalyst reducibility was studied by temperature programmed reduction analysis (TPR) in a Micromeritics Autochem 2910 equipment by flowing a reducing mixture (10% H_2/Ar) through the sample while heating up to 980 °C using a heating rate of 5 °C/min. Carbon deposited after oxidative steam reforming reaction was analyzed by thermogravimetric analysis (TGA) over the used catalysts on a TGA-DSC Mettler Toledo thermobalance in air flow with a heating rate of 5 °C/min up to 1000 °C. Finally, the morphology of the used samples was evaluated by transmission electron microscopy (TEM) at the National Centre for Electron Microscopy (CNME, Complutense University of Madrid), using a JEOL JEM 2100 microscope (200 kV) with a resolution of 0.25 nm.

Catalytic tests

Acetic acid oxidative steam reforming reactions were isothermally performed at 500 °C and atmospheric pressure in a fixed-bed reactor on a Microactivity-Pro unit described before [17]. Previously, the catalysts were reduced under pure hydrogen according to H_2-TPR results at 600 °C. After that, a nitrogen stream flowed into the reactor to achieve the desired reaction conditions. Then, a mixture of acetic acid and water (steam-to-carbon = 2) was pumped to the reactor at a WHSV of 15 h^{-1}, defined as the ratio between the liquid feed mass flowrate and the mass of catalyst used. The oxygen-nitrogen gas mixture composition allows us to work with an O_2/AcOH molar ratio of 0.15 whit a total gas flow of 60 mL/min.

The reactor outlet stream was evaluated by using an Agilent 490 Micro-GC equipped with a thermal conductivity detector (TCD), a Pora Plot U column (10 m), and a Molecular Sieve 5A column (20 m) which allow the online determination of the product gas stream composition. A Varian CP-3900 chromatograph equipped with an Agilent J&W CP-WAX 52 CB column and flame ionization detector (FID) was used to analyze the condensable vapors previously trapped in a condenser at 4 °C. 1,4-butanediol was used as an internal standard.

The catalytic performance was evaluated in terms of acetic acid conversion (X_{AcOH}, Equation (2)), hydrogen yield (Y_{H2}, Equation (3)), and carbon co-products selectivities (S_{CO}, S_{CO2}, S_{CH4}, Equation (4)), where F is related to the molar flowrate at the inlet (in) or the outlet (out) of the reactor.

$$X_{AcOH} = \frac{F_{AcOH,in} - F_{AcOH,out}}{F_{AcOH,in}} \cdot 100 \quad (2)$$

$$Y_{H_2} = \frac{F_{H_2,out}}{4 \cdot F_{AcOH,in}} \cdot 100 \quad (3)$$

$$S_i = \frac{F_{i,out}}{2 \cdot (F_{AcOH,in} - F_{AcOH,out})} \cdot 100 \quad (4)$$

The value of carbon deposited during the reaction is given as:

$$Coke\left(mg_{coke} \cdot g_{cat}{}^{-1} \cdot h^{-1}\right) = \frac{m_{coke}(mg)}{m_{catalyst}(g) \cdot TOS(h)} \cdot 100 \quad (5)$$

whereas m_{coke} is the amount of coke deposited along the reaction and, $m_{catalyst}$ is the amount of catalyst loaded into the reactor (0.3 g).

Results and discussion

Characterization of the prepared catalysts

Firstly, the bare supports, SBA-15 and CeO_2-m, were characterized by TEM to verify the porous mesostructure achieved during the synthesis. In this regard, the micrographs of the calcined samples are displayed in Fig. 1. SBA-15 (Fig. 1A) shows the hexagonal mesoporous structure typical for this material. On the other hand, CeO_2-m (Fig. 1B) shows an aligned nanorods structure. These elongated structures are formed by small rounded CeO_2 particles replicating the unidirectional channels of the SBA-15 used as hard-template.

The physicochemical properties of the supports and the corresponding catalysts used in this work are summarized in Table 1. As it can be discerned from the values, metal loadings determined by ICP-AES analysis are close to the fixed during the synthesis.

Fig. 2 displays the N_2-physisorption isotherms at 77 K. SBA-15 and CeO_2-m-based samples showed type IV isotherms with an H1-type and H3-type hysteresis loop, respectively, according to the IUPAC classification. The H1-type hysteresis loop is ascribed to a narrow range of uniform hexagonal mesoporous structures, whereas the H3-type is ascribed to materials with slit-shaped pores [31] as a consequence of the porous structure obtained by nanocasting. After the support modification with La_2O_3 and Ni incorporation (Fig. 2B), the isotherm shapes are similar to those of the corresponding supports (Fig. 2A) but shifted to lower N_2 adsorption volumes. This corroborates the preservation of the initial mesoporous structure of supports in the final catalysts. By applying the Brunauer, Emmett, and Teller (BET) method, the surface areas were obtained, included in Table 1. In both cases, the BET surface area decreases when increasing the metal content, which evidences the presence of oxide nanoparticles within the porous structure. Whereas SBA-15-based samples reached higher specific surface areas, CeO_2-m samples achieved values considerably smaller given the differences between the density of the bulk phases and the different porous structures. However, these results are comparable to those reported by other authors with similar materials when using SBA-15 as hard-template [32,33].

To study the reducibility of the catalysts, H_2-TPR measurements were carried out on the calcined samples. The reduction profiles of the four catalysts are shown in Fig. 3. Ni SBA-15 profile shows reduction in a wide temperature range with two features at 411 °C and 516 °C ascribed to the reduction of Ni^{2+} species with different interaction degrees. The higher temperature zone corresponds to Ni-phase interacting more strongly with the support [34,35]. The addition of La_2O_3 to Ni/SBA-15 shifted the reduction profile towards higher temperatures (around 600 °C) indicating a stronger metal-support interaction according to the results reported by Wang et al. [36]. In the case of Ni/CeO_2-m, the main reduction zone is located in the temperature range of 300–450 °C related to the reduction of NiO into Ni^0. On the other hand, another peak arises at higher temperatures (755 °C) ascribed to the partial reduction of bulk CeO_2 [37]. Ni/La_2O_3–CeO_2-m presents the main reduction zone shifted to higher temperatures

Please cite this article as: Megía PJ et al., Oxidative steam reforming of acetic acid on Ni catalysts: Influence of the La promotion on mesostructured supports, International Journal of Hydrogen Energy, https://doi.org/10.1016/j.ijhydene.2023.06.283

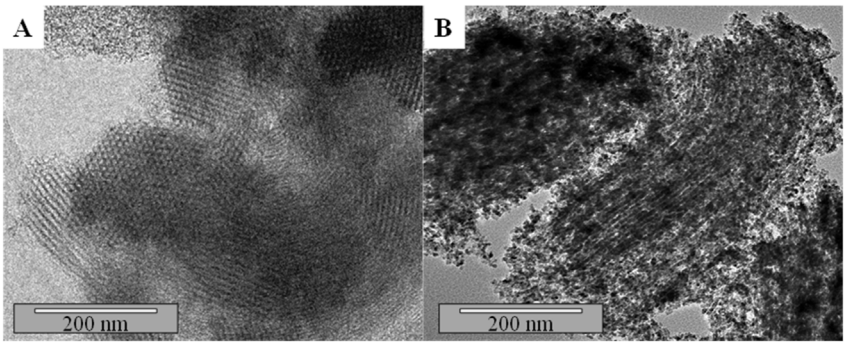

Fig. 1 – TEM micrographs of calcined (A) SBA-15, (B) CeO_2-m.

compared to the non-promoted sample, suggesting that NiO remains in more intimate contact with the support [38]. This effect is due to the ability of La_2O_3 to act as a structural promoter which prevents the aggregation of Ni particles during the reduction [39] thus allowing a higher surface of interaction between the Ni-phase and CeO_2. However, the peak at higher temperatures which was previously ascribed to the partial reduction of ceria, is shifted to lower temperatures suggesting that La-promotion enhances ceria reducibility as reported by Pizzolitto et al. [40].

After the activation at 600 °C, samples were characterized by X-ray diffraction. The obtained diffractograms for the reduced catalysts are shown in Fig. 4. Since no diffraction lines of NiO could be distinguished the reduction step was successful. On the contrary, peaks corresponding to the metallic nickel pattern with a cubic crystal system (JCPDS 01-071-3740) arise, a good indicator that the reduction step was successful. Regarding SBA-15-based samples, Ni/SBA-15 showed diffraction at $2\theta = 44.5$, 51.8, and 76.4° ascribed to Ni^0. After the La_2O_3 promotion, only the first signal could be differentiated, confirming that the presence of La_2O_3 prevents the aggregation of Ni particles. In addition, no diffraction lines of lanthanum oxide could be appreciated thus, tiny particles beyond the detection limit of the equipment (3 nm) were formed, indicating that La is distributed in sheet form over the support [41], thus facilitating the contact with Ni species. On the other hand, Ni/CeO_2-m showed diffraction lines of metallic Ni at $2\theta = 44.5$ and, 51.8° along with those of cubic CeO_2 at $2\theta = 28.3$, 32.8, 47.2, 56.0, 58.9, 69.2, 76.4, and 78.9° (JCPDS 01-089-8436). Given that Ce-oxides require temperatures above 1000 °C to be reduced, they remain as oxide after the activation process (600 °C) and no diffraction lines of metallic Ce appear [42]. Similarly to Ni/La_2O_3-SBA-15, in Ni/La_2O_3–CeO_2-m no diffraction lines of La_2O_3 could be distinguished. In general, due to the presence of La_2O_3 in the carrier, the pattern of Ni/La_2O_3-SBA-15 and Ni/La_2O_3–CeO_2-m display broader Ni diffraction peaks. Based on this, it is reasonable that the mean crystallite sizes calculated by applying the Debye-Scherrer equation on the reflection peak (111) of the cubic Ni^0 pattern are smaller than the non-promoted samples (see Table 1).

Catalytic activity in the oxidative steam reforming of acetic acid

In order to investigate the performance of the Ni-based catalysts in the oxidative steam reforming to compare the effect of the support nature and lanthanum promotion, their catalytic activity was evaluated in terms of acetic acid conversion and hydrogen yield with time on stream. The obtained results are shown in Fig. 5. It is possible to observe that the Ni/CeO_2-m sample achieved better catalytic behavior than Ni/SBA-15. This sample reached almost complete conversion and

Table 1 – Physicochemical properties of supports and Ni catalysts.

Sample	Ni[a] (wt.%)	La[a] (wt.%)	S_{BET} (m^2/g)	Vp[b] (cm^3/g)	Dp[c] (nm)	D_{Ni}[d] (nm)
SBA-15	–	–	601	0.91	7.7	–
Ni/SBA-15	6.5	–	533	0.80	7.8	11.5 ± 0.4
La_2O_3-SBA-15	–	9.6	474	0.76	7.7	–
Ni/La_2O_3-SBA-15	6.2	9.4	407	0.63	7.3	4.6 ± 0.3
CeO_2-m	–	–	114	0.29	7.3	–
Ni/CeO_2-m	6.7	–	98	0.26	8.1	7.6 ± 0.3
La_2O_3–CeO_2-m	–	9.1	86	0.22	8.2	–
Ni/La_2O_3–CeO_2-m	6.5	9.0	73	0.17	8.1	5.7 ± 0.2

[a] Obtained by ICP-AES.
[b] Determined at $P/P_0 = 0.95$.
[c] Maximum BJH pore size distribution.
[d] Calculated from the reflection peak (111) of Ni.[0] pattern in the reduced materials using the Debye-Scherrer equation.

Please cite this article as: Megía PJ et al., Oxidative steam reforming of acetic acid on Ni catalysts: Influence of the La promotion on mesostructured supports, International Journal of Hydrogen Energy, https://doi.org/10.1016/j.ijhydene.2023.06.283

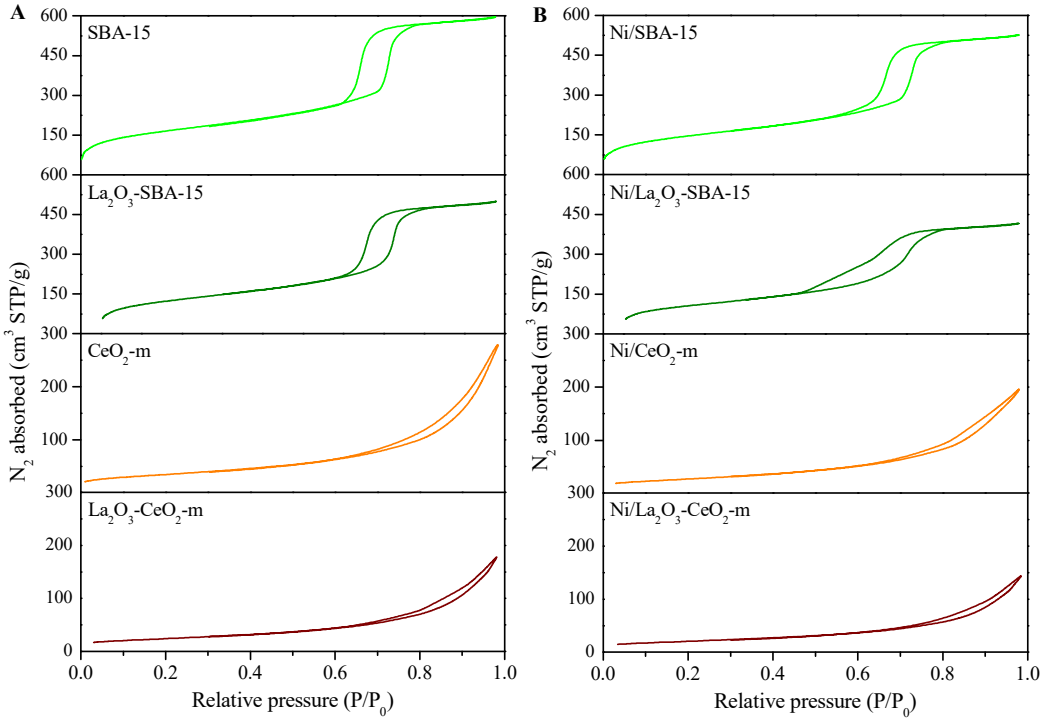

Fig. 2 – N_2 adsorption-desorption isotherms of calcined supports (A) and catalysts (B) at 77K.

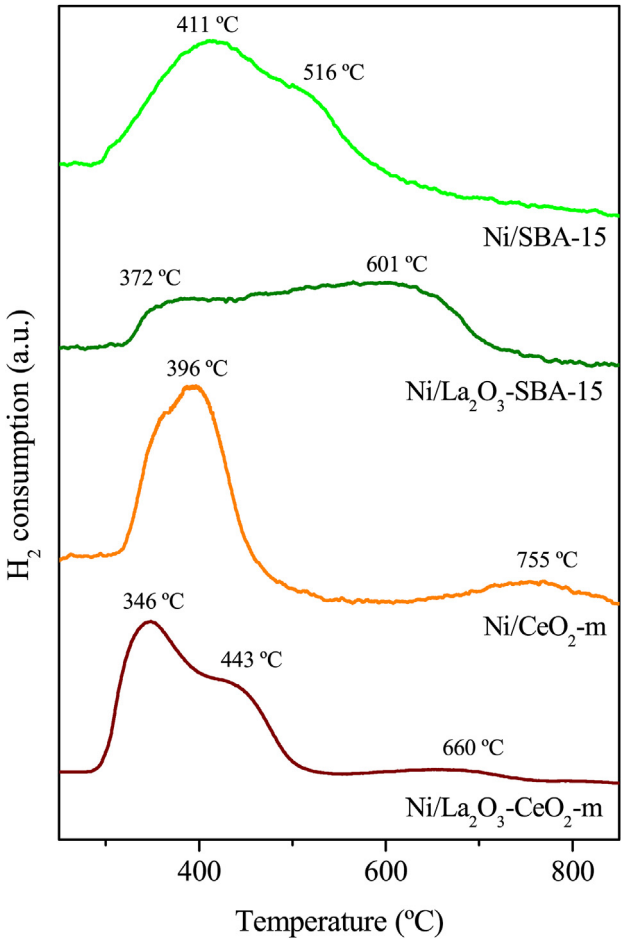

Fig. 3 – TPR profiles of calcined catalysts.

hydrogen yields over 46% after 5 h time on stream. On the contrary, Ni/SBA-15 suffered severe deactivation during the test, decreasing both acetic acid conversion and hydrogen yield down to 28% and 17%, respectively. Despite it has been widely reported as a carrier for conventional steam reforming of different oxygenates [43–45], bare SBA-15 is not an adequate support of Ni catalysts in an oxidizing environment as evidenced by these results. However, regarding the effect of lanthanum promotion, Ni/La_2O_3-SBA-15 tripled the conversion value for 5 h while the hydrogen yield became 2.4 higher compared to Ni/SBA-15 sample. This effect is related to

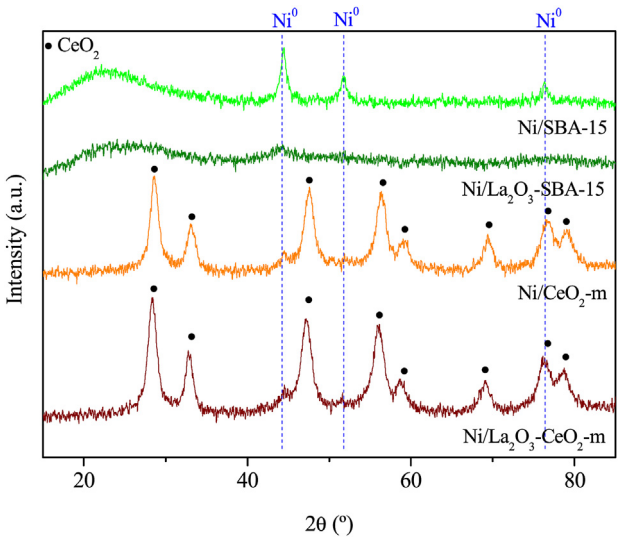

Fig. 4 – XRD diffraction patterns of catalysts reduced at 600 °C.

Please cite this article as: Megía PJ et al., Oxidative steam reforming of acetic acid on Ni catalysts: Influence of the La promotion on mesostructured supports, International Journal of Hydrogen Energy, https://doi.org/10.1016/j.ijhydene.2023.06.283

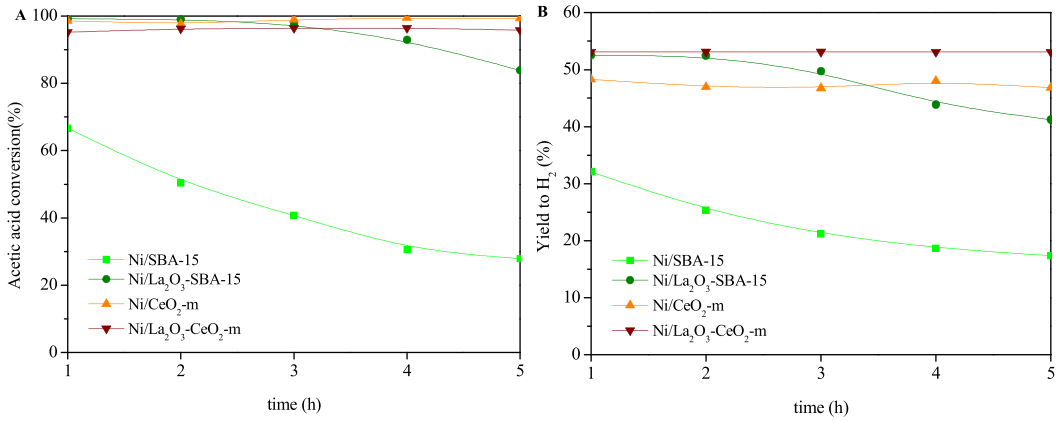

Fig. 5 – Evolution of acetic acid conversion (A) and hydrogen yield (B) with time on stream at 500 °C for Ni/SBA-15, Ni/La_2O_3-SBA-15, Ni/CeO_2-m, and Ni/La_2O_3–CeO_2-m catalysts (S/C = 2, O_2/AcOH = 0.15).

smaller crystallite size (see Table 1) given the ability of La_2O_3 to act as a dispersing promoter preventing the aggregation of Ni particles [46,47]. On the other hand, the La_2O_3 addition to Ni/CeO_2-m resulted in a similar acetic acid conversion with an increase of about 6% in the hydrogen yield. Given that the calculated crystallite size for both promoted samples was similar, the superior catalytic activity in the oxidative steam reforming of acetic acid obtained with Ni/La_2O_3–CeO_2-m is not only related to higher dispersion but also to the presence of CeO_2 in the carrier which is active in the water-gas shift reaction and promotes coke gasification due its capacity to store/release oxygen [20].

Apart from these results, other products were detected in the gas outlet stream. In this regard, the selectivities for CH_4, CO, and CO_2 after 5 h time on stream are summarized in Table 2. As it is reported in the literature, lower methane selectivity is associated with higher hydrogen production [48]. This assumption is entirely in line with the results obtained for Ni/CeO_2-m and Ni/La_2O_3–CeO_2-m. However, SBA-15-supported samples did not follow the same trend. As reported elsewhere [49], during the acetic acid steam reforming, methane and carbon dioxide (deriving from the acetic acid decomposition) are intermediates appearing in the first stage of the steam reforming pathway. Thus, the lower methane selectivity for Ni/SBA-15 could be related to the low acetic acid conversion achieved with this sample. In the same way, methane yield is also lower for Ni/SBA-15, 2.63% versus 11.61% for Ni/La_2O_3-SBA-15. In that scenario, the low amount of methane produced through acetic acid decomposition would be easily reformed towards hydrogen in the available active sites. Attending to CO and CO_2, the presence of ceria in the carrier resulted in a higher S_{CO2}/S_{CO} ratio since it promotes the water-gas shift reaction [20,50] given the oxygen exchange capacity due to the Ce^{4+}/Ce^{3+} redox couple.

To shed light on the differences observed in the catalytic performance during the oxidative steam reforming of acetic acid, the spent catalysts were characterized by means of XRD, TGA, and TEM. The diffractogram patterns of the used catalysts after 5 h time on stream are shown in Fig. 6. Features ascribed to graphitic carbon (JCPDS 00-041-1487) at $2\theta = 25.5$ and 54.4° could be discerned associated with the (002) and (100) planes, respectively. These diffraction lines proved the coke deposition being more pronounced for SBA-15-based materials suggesting that higher carbon formation is taking place along the reaction. On the other hand, peaks corresponding to the cubic phase of Ni^0 (JCPDS 01-071-3740) arise in all the samples (JCPDS 01-071-3740). It is noteworthy how apart from the metallic nickel features, on Ni/SBA-15 the presence of NiO (JCPDS 01-075-0197) with a cubic crystal system is evident at $2\theta = 43.2$, and 62.9°. In context, apart from coke deposition, the active phase is being oxidized leading to non-active sites which could explain the poor catalytic activity obtained during the tests (see Fig. 5). It should be noted that sintering can also take place thus, decreasing the Ni^0 dispersion which could not be recovered [10]. By applying the Debye-Scherrer equation on the main diffraction line of the Ni^0

Table 2 – Gas product selectivities, mean Ni^0 crystallite size of spent catalysts, and coke deposition on the acetic acid oxidative steam reforming using mesostructured Ni-based catalysts.

Sample	Gas products selectivities			D_{Ni}[a]	Coke deposited[b]
	CH_4 (mol%)	CO (mol%)	CO_2 (mol%)	(nm)	($mg_{coke} \cdot g_{cat}^{-1} \cdot h^{-1}$)
Ni/SBA-15	9.5	12.0	78.5	14.7 ± 0.5	173.5
Ni/La_2O_3-SBA-15	13.8	8.7	77.5	4.4 ± 0.3	223.5
Ni/CeO_2-m	10.4	6.6	83.0	10.4 ± 0.4	117.1
Ni/La_2O_3–CeO_2-m	6.6	7.8	85.6	5.8 ± 0.2	62.3

[a] Calculated from the reflection peak (111) of Ni^0 pattern in the used catalysts using the Debye-Scherrer equation.
[b] Estimated by TGA in airflow.

Please cite this article as: Megía PJ et al., Oxidative steam reforming of acetic acid on Ni catalysts: Influence of the La promotion on mesostructured supports, International Journal of Hydrogen Energy, https://doi.org/10.1016/j.ijhydene.2023.06.283

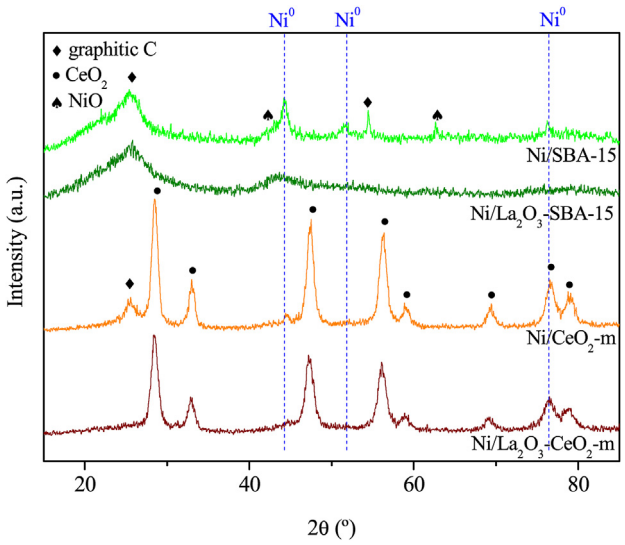

Fig. 6 – XRD diffraction patterns of the used catalysts after 5 h time on stream.

pattern ($2\theta = 44.5°$) is possible to calculate the mean crystallite size after the reaction. The obtained results are summarized in Table 2. Comparing the obtained results for Ni^0 particles in the spent catalysts with those obtained for the reduced samples (see Table 1), it can be assured that sintering is taking place in the non-promoted La_2O_3 samples since the mean crystallite size increase of about 30% for Ni/SBA-15 and Ni/CeO_2-m catalysts after 5 h time on stream. On the contrary, the La_2O_3 addition prevented sintering as the mean crystallite sizes remained almost constant as reported before [26]. To estimate the amount of coke deposited during the reaction, TGA analyses were performed on the used catalysts. The amount of coke formed during the oxidative steam reforming reaction is displayed in Table 2. As expected, the samples supported over CeO_2 achieved much lower coke deposition than SBA-15-supported samples ascribed to its ability to promote coke gasification [20]. On the other hand, the La-promotion to Ni/CeO_2-m decreased 53% in the coke deposition. Given that the conversion values were similar for both, Ni/CeO_2-m and Ni/La_2O_3–CeO_2-m, this effect is ascribed to lanthanum's ability to prevent the aggregation of Ni particles [39] resulting in higher dispersion and higher oxygen mobility [51]. Large Ni particles have been reported to promote coke formation [41], which supports the obtained results. However, this effect could not be appreciated for SBA-15-based materials. According to the catalytic results, this could be related to the higher acetic acid conversion reached with Ni/La_2O_3-SBA-15 which may lead to higher coke formation. As discussed above, acetic acid decomposition could lead to methane and coke production which agrees with product distribution observed with Ni/La_2O_3-SBA-15 where higher methane yield and coke deposition were observed.

Finally, to further characterize the coke deposition, TEM and differential thermogravimetric (DTG) techniques were performed on the used samples. TEM micrographs are displayed in Fig. 7. The well-ordered hexagonal mesoporous structure was maintained concerning Ni/SBA-15 and Ni/La_2O_3-SBA-15. However, the ordered structure of CeO_2 disappeared probably due to the operating conditions or to the growth of carbon nanofiber during the reaction. Despite this, Ni/CeO_2-m and Ni/La_2O_3–CeO_2-m maintained a good catalytic performance. This demonstrates that although the porous mesostructure of the support is important to get a high Ni dispersion [30], this structure seems not to be essential to maintain the catalytic activity. Concerning coke deposition, in general, filamentous coke with different ordering degrees can be distinguished in all the samples. This assumption aligns with the results obtained from DTG curves, which are displayed in Fig. 8. Overall, all the samples show a maximum at temperatures between 450 and 550 °C which evidence the formation of carbon nanofilaments with different ordering

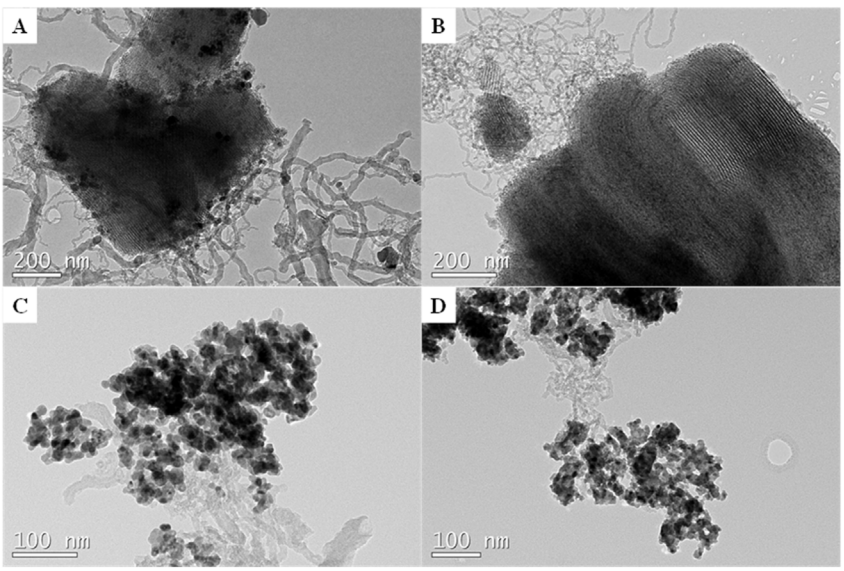

Fig. 7 – TEM micrographs of used (A) Ni/SBA-15, (B) Ni/La_2O_3-SBA-15, (C) Ni/CeO_2-m, and (D) Ni/La_2O_3–CeO_2-m Catalysts after 5 h time on stream.

Please cite this article as: Megía PJ et al., Oxidative steam reforming of acetic acid on Ni catalysts: Influence of the La promotion on mesostructured supports, International Journal of Hydrogen Energy, https://doi.org/10.1016/j.ijhydene.2023.06.283

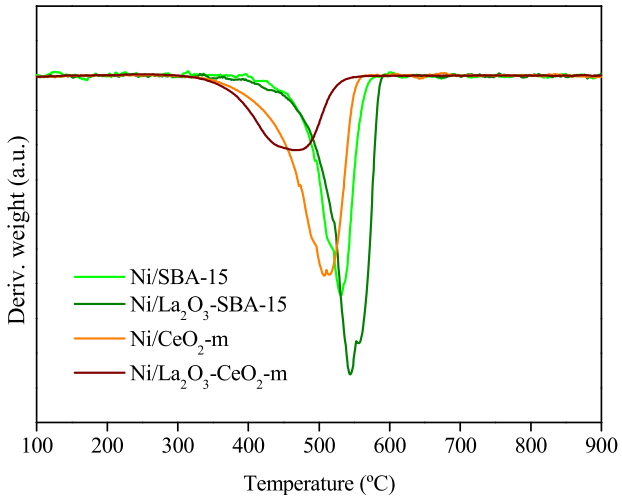

Fig. 8 – DTG profiles of the used catalysts after 5 h time on stream.

degrees since amorphous carbon would oxidize at temperatures below 400 °C [7,52]. It is noteworthy how adding La_2O_3 to CeO_2-m leads to a reduction in the oxidation temperature of coke ascribed to the increase in oxygen vacancies which would facilitate the oxygen transfer to carbon as reported elsewhere [47]. However, this effect was not observed for SBA-15 supported samples. Reviewing the literature, other authors reported several trends in the evolution of coke oxidation temperature after lanthanum incorporation into the catalyst. In this regard, Kiani et al. [53] reported that adding La_2O_3 to SBA-16 led to an enhancement in coke thermal stability compared to the non-promoted sample.

Conclusions

The effect of the support nature and the La-promotion on the catalytic performance of the oxidative steam reforming of acetic acid using Ni as the active phase was investigated for the first time. The obtained results when using SBA-15 or mesoporous CeO_2 as a carrier revealed that bare SBA-15 is not suitable to be used as support for Ni catalysts in an oxidizing environment, as evidenced by the active phase oxidation, which may explain the low conversion and hydrogen yield reached. However, using mesoporous CeO_2 due to its ability to store/release oxygen, led to almost complete conversion (>97%) and higher hydrogen yields (~47%) than those obtained with SBA-15.

La_2O_3 addition to the support led to an increase in Ni dispersion as evidenced by the mean crystallite size calculated through the Debye-Scherrer equation in the reduced samples. This effect was more pronounced when using SBA-15. Consequently, the conversion and the hydrogen selectivity for Ni/La_2O_3-SBA-15 were 3 and 2.4 times higher, respectively, than for the non-promoted sample. Moreover, the presence of lanthanum in SBA-15 and CeO_2-m hindered the sintering effect during the test as the mean crystallite size remained constant after 5 h time on stream.

However, due to the convergence between small crystallites sizes and the high oxygen mobility of ceria, Ni/La_2O_3–CeO_2-m achieved the best catalytic performance with high acetic acid conversion (~96%), the highest hydrogen yield (~53%) close to the expected value in the thermodynamic equilibrium, and the lowest coke formation (62.3 $mg_{coke} \cdot g_{cat}^{-1} \cdot h^{-1}$).

Funding

The authors gratefully acknowledge the financial support from the Community of Madrid (project S2018/EMT-4344), and the Spanish Ministry for Science and Innovation (project PID2020-117273RB-I00).

Declaration of competing interest

The authors declare that they have no known competing financial interests or personal relationships that could have appeared to influence the work reported in this paper.

REFERENCES

[1] Uddin MN, Techato K, Taweekun J, Rahman MM, Rasul MG, Mahlia TMI, et al. An overview of recent developments in biomass pyrolysis technologies. Energies 2018;11:3115. https://doi.org/10.3390/en11113115.
[2] Megía PJ, Vizcaíno AJ, Calles JA, Carrero A. Hydrogen production technologies: from fossil fuels toward renewable sources. A mini review. Energy Fuel 2021;35:16403–15. https://doi.org/10.1021/acs.energyfuels.1c02501.
[3] Pal DB, Singh A, Bhatnagar A. A review on biomass based hydrogen production technologies. Int J Hydrogen Energy 2022;47:1461–80. https://doi.org/10.1016/J.IJHYDENE.2021.10.124.
[4] McKendry P. Energy production from biomass (part 1): overview of biomass. Bioresour Technol 2002;83:37–46. 10.1016/S0960-8524(01)00118-3.
[5] Katakojwala R, Kopperi H, Kumar S, Venkata Mohan S. Hydrothermal liquefaction of biogenic municipal solid waste under reduced H2 atmosphere in biorefinery format. Bioresour Technol 2020;310:123369. https://doi.org/10.1016/j.biortech.2020.123369.
[6] Sipra AT, Gao N, Sarwar H. Municipal solid waste (MSW) pyrolysis for bio-fuel production: a review of effects of MSW components and catalysts. Fuel Process Technol 2018;175:131–47. https://doi.org/10.1016/j.fuproc.2018.02.012.
[7] Megía PJ, Vizcaíno AJ, Ruiz-Abad M, Calles JA, Carrero A. Coke evolution in simulated bio-oil aqueous fraction steam reforming using Co/SBA-15. Catal Today 2021:367. https://doi.org/10.1016/j.cattod.2020.04.069.
[8] García-Gómez N, Valecillos J, Valle B, Remiro A, Bilbao J, Gayubo AG. Combined effect of bio-oil composition and temperature on the stability of Ni spinel derived catalyst for hydrogen production by steam reforming. Fuel 2022;326:124966. https://doi.org/10.1016/j.fuel.2022.124966.
[9] Setiabudi HD, Aziz MAA, Abdullah S, Teh LP, Jusoh R. Hydrogen production from catalytic steam reforming of biomass pyrolysis oil or bio-oil derivatives: a review. Int J Hydrogen Energy 2020;45. 10.1016/j.ijhydene.2019.10.141.
[10] Arandia A, Remiro A, Valle B, Bilbao J, Gayubo AG. Deactivation of Ni spinel derived catalyst during the

oxidative steam reforming of raw bio-oil. Fuel 2020;276:117995. https://doi.org/10.1016/j.fuel.2020.117995.
[11] Palma V, Ruocco C, Ricca A. Oxidative steam reforming of ethanol in a fluidized bed over CeO2-SiO2 supported catalysts: effect of catalytic formulation. Renew Energy 2018;125:356–64. https://doi.org/10.1016/J.RENENE.2018.02.118.
[12] Moreira R, Bimbela F, Gandía LM, Ferreira A, Sánchez JL, Portugal A. Oxidative steam reforming of glycerol. A review. Renew Sustain Energy Rev 2021;148. https://doi.org/10.1016/j.rser.2021.111299.
[13] Nahar G, Dupont V. Recent advances in hydrogen production via autothermal reforming process (ATR): a review of patents and research articles. Recent Pat Chem Eng 2013;6:8–42. https://doi.org/10.2174/2211334711306010003.
[14] Haynes DJ, Shekhawat D. Oxidative steam reforming. Fuel Cells Technol Fuel Process 2011;129–90. https://doi.org/10.1016/B978-0-444-53563-4.10006-9.
[15] Veiga S, Romero M, Faccio R, Segobia D, Duarte H, Apesteguía C, et al. Hydrogen-rich gas production by steam and oxidative steam reforming of crude glycerol over Ni-La-Me mixed oxide catalysts (Me= Ce and/or Zr). Catal Today 2020;344:190–8. https://doi.org/10.1016/J.CATTOD.2019.02.008.
[16] Ibrahim SA, Ekinci EK, Karaman BP, Oktar N. Coke-resistance enhancement of mesoporous γ-Al2O3 and MgO-supported Ni-based catalysts for sustainable hydrogen generation via steam reforming of acetic acid. Int J Hydrogen Energy 2021;46:38281–98. https://doi.org/10.1016/J.IJHYDENE.2021.09.084.
[17] Megía PJ, Carrero A, Calles JA, Vizcaíno AJ. Hydrogen production from steam reforming of acetic acid as a model compound of the aqueous fraction of microalgae HTL using Co-M/SBA-15 (M: Cu, Ag, Ce, Cr) catalysts. Catalysts 2019;9:1013. https://doi.org/10.3390/catal9121013.
[18] Chen Y, Huang Y. Influence of ceria existence form on deactivation behavior of Cu-Ce/SBA-15 catalysts for methanol steam reforming. Int J Hydrogen Energy 2022. https://doi.org/10.1016/J.IJHYDENE.2022.10.046.
[19] Abdullah N, Ainirazali N, Ellapan H. Structural effect of Ni/SBA-15 by Zr promoter for H2 production via methane dry reforming. Int J Hydrogen Energy 2021;46:24806–13. https://doi.org/10.1016/J.IJHYDENE.2020.07.060.
[20] Osorio-Vargas P, Flores-González NA, Navarro RM, Fierro JLG, Campos CH, Reyes P. Improved stability of Ni/Al2O3 catalysts by effect of promoters (La2O3, CeO2) for ethanol steam-reforming reaction. Catal Today 2016;259:27–38. https://doi.org/10.1016/j.cattod.2015.04.037.
[21] Wang H, Zhu H, Zhang Y, Pu J. Highly active Ni/CeO2 for the steam reforming of acetic acid using CTAB as surfactant template. Int J Hydrogen Energy 2022;47:27493–507. https://doi.org/10.1016/J.IJHYDENE.2022.06.072.
[22] Vizcaíno AJ, Carrero A, Calles JA. Hydrogen production by ethanol steam reforming over Cu–Ni supported catalysts. Int J Hydrogen Energy 2007;32:1450–61. https://doi.org/10.1016/J.IJHYDENE.2006.10.024.
[23] Muñoz M, Moreno S, Molina R. Promoting effect of Ce and Pr in Co catalysts for hydrogen production via oxidative steam reforming of ethanol. Catal Today 2013;213:33–41. https://doi.org/10.1016/J.CATTOD.2013.04.037.
[24] Megía PJ, Calles JA, Carrero A, Vizcaíno AJ. Effect of the incorporation of reducibility promoters (Cu, Ce, Ag) in Co/CaSBA-15 catalysts for acetic acid steam reforming. Int J Energy Res 2021;45:1685–702. https://doi.org/10.1002/er.5832.
[25] Balopi B, Moyo M, Gorimbo J. Autothermal reforming of bio-ethanol: a short review of strategies used to synthesize coke-resistant nickel-based catalysts. Catal Lett 2022;1:1–13. https://doi.org/10.1007/S10562-021-03892-2.
[26] Carrero A, Vizcaíno AJ, Calles JA, García-Moreno L. Hydrogen production through glycerol steam reforming using Co catalysts supported on SBA-15 doped with Zr, Ce and La. J Energy Chem 2017;26:42–8. https://doi.org/10.1016/j.jechem.2016.09.001.
[27] Charisiou ND, Siakavelas G, Papageridis KN, Baklavaridis A, Tzounis L, Polychronopoulou K, et al. Hydrogen production via the glycerol steam reforming reaction over nickel supported on alumina and lanthana-alumina catalysts. Int J Hydrogen Energy 2017;42:13039–60. https://doi.org/10.1016/J.IJHYDENE.2017.04.048.
[28] Guo W, Li G, Zheng Y, Li K, Guo L. Influence of La2O3 addition on activity and coke formation over Ni/SiO2 for acetic acid steam reforming. Int J Hydrogen Energy 2022;47:3633–43. https://doi.org/10.1016/J.IJHYDENE.2021.11.023.
[29] Zhao D, Feng J, Huo Q, Melosh N, Fredrickson GH, Chmelka BF, et al. Triblock copolymer syntheses of mesoporous silica with periodic 50 to 300 angstrom pores. Science 1998;279:548–52. https://doi.org/10.1126/science.279.5350.548. 80-.
[30] Megía PJ, Morales A, Vizcaíno AJ, Calles JA, Carrero A. Hydrogen production through oxidative steam reforming of acetic acid over Ni catalysts supported on ceria-based materials. Catal 2022;12:1526. https://doi.org/10.3390/CATAL12121526. 2022;12:1526.
[31] Sing KSW, Everett DH, Haul RAW, Moscou L, Pierotti RA, Rouquerol J, et al. Reporting physisorption data for gas/solid systems with special reference to the determination of surface area and porosity. Pure Appl Chem 1985;57:603–19. https://doi.org/10.1351/pac198557040603.
[32] Roggenbuck J, Schäfer H, Tsoncheva T, Minchev C, Hanss J, Tiemann M. Mesoporous CeO2: synthesis by nanocasting, characterisation and catalytic properties. Microporous Mesoporous Mater 2007;101:335. https://doi.org/10.1016/J.MICROMESO.2006.11.029. 341.
[33] Luo L, Oliver CC, Joseph IM, Gang DD, Chen M, Hernandez R, et al. Pore structure of ordered mesoporous Pt-CeO2 probed by CO via VT-DRIFTS. Appl Surf Sci 2022;588:152866. https://doi.org/10.1016/J.APSUSC.2022.152866.
[34] Carrero A, Calles JA, García-Moreno L, Vizcaíno AJ. Production of renewable hydrogen from glycerol steam reforming over bimetallic Ni-(Cu,Co,Cr) catalysts supported on SBA-15 silica. Catalysts 2017;7. https://doi.org/10.3390/catal7020055.
[35] Ruocco C, Cortese M, Martino M, Palma V. Fuel grade bioethanol reforming in a fluidized bed reactor over highly durable Pt-Ni/CeO2-SiO2 catalysts. Chem Eng Process - Process Intensif 2022;174:108888. https://doi.org/10.1016/J.CEP.2022.108888.
[36] Wang X, Zhu L, Zhuo Y, Zhu Y, Wang S. Enhancement of CO2 methanation over La-modified Ni/SBA-15 catalysts prepared by different doping methods. ACS Sustainable Chem Eng 2019;7:14647–60. https://doi.org/10.1021/ACSSUSCHEMENG.9B02563.
[37] Kun-udom R, Jantarang S, Du Z, Kitiyanan B, Rirksomboon T, Meeyoo V. Morphology dependent? Elucidating the catalyst structures of Ni/Ce0.75Zr0.25O2 in the steam reforming of acetic acid. Green Chem Eng 2022;3:44–54. https://doi.org/10.1016/J.GCE.2021.08.004.
[38] Greluk M, Rotko M, Turczyniak-Surdacka S. Enhanced catalytic performance of La2O3 promoted Co/CeO2 and Ni/CeO2 catalysts for effective hydrogen production by ethanol steam reforming. Renew Energy 2020;155:378–95. https://doi.org/10.1016/j.renene.2020.03.117.
[39] Mo W, Ma F, Ma Y, Fan X. The optimization of Ni–Al2O3 catalyst with the addition of La2O3 for CO2–CH4 reforming to produce syngas. Int J Hydrogen Energy 2019;44:24510–24. https://doi.org/10.1016/J.IJHYDENE.2019.07.204.

Please cite this article as: Megía PJ et al., Oxidative steam reforming of acetic acid on Ni catalysts: Influence of the La promotion on mesostructured supports, International Journal of Hydrogen Energy, https://doi.org/10.1016/j.ijhydene.2023.06.283

[40] Pizzolitto C, Menegazzo F, Ghedini E, Innocenti G, Di Michele A, Cruciani G, et al. Increase of ceria redox ability by lanthanum addition on Ni based catalysts for hydrogen production. ACS Sustainable Chem Eng 2018;6:13867–76. https://doi.org/10.1021/acssuschemeng.8b02103.
[41] Calles JA, Carrero A, Vizcaíno AJ. Ce and La modification of mesoporous Cu–Ni/SBA-15 catalysts for hydrogen production through ethanol steam reforming. Microporous Mesoporous Mater 2009;119:200–7. https://doi.org/10.1016/J.MICROMESO.2008.10.028.
[42] Scheffe JR, Steinfeld A. Thermodynamic analysis of cerium-based oxides for solar thermochemical fuel production. Energy Fuel 2012;26:1928–36. https://doi.org/10.1021/ef201875v.
[43] Calles JA, Carrero A, Vizcaíno AJ, García-Moreno L, Megía PJ. Steam reforming of model bio-oil aqueous fraction using Ni-(Cu, Co, Cr)/SBA-15 catalysts. Int J Mol Sci 2019;20. https://doi.org/10.3390/ijms20030512.
[44] Zhang Z, Hu X, Zhang L, Yang Y, Li Q, Fan H, et al. Steam reforming of guaiacol over Ni/Al2O3 and Ni/SBA-15: impacts of support on catalytic behaviors of nickel and properties of coke. Fuel Process Technol 2019;191:138–51. https://doi.org/10.1016/J.FUPROC.2019.04.001.
[45] Haocui Z, Zhourong X, Mei Y, Yajie T, Guozhu L, Xiangwen Z, et al. Catalytic steam reforming of JP-10 over Ni/SBA-15. Int J Hydrogen Energy 2020;45:4284–96. https://doi.org/10.1016/J.IJHYDENE.2019.12.049.
[46] Araújo JCS, Oton LF, Bessa B, Neto ABS, Oliveira AC, Lang R, et al. The role of Pt loading on La2O3-Al2O3 support for methane conversion reactions via partial oxidation and steam reforming. Fuel 2019;254:115681. https://doi.org/10.1016/J.FUEL.2019.115681.
[47] Moogi S, Lee IG, Hwang KR. Catalytic steam reforming of glycerol over Ni–La2O3–CeO2/SBA-15 catalyst for stable hydrogen-rich gas production. Int J Hydrogen Energy 2020;45:28462–75. https://doi.org/10.1016/J.IJHYDENE.2020.07.249.
[48] Niazi Z, Irankhah A, Wang Y, Arandiyan H. Cu, Mg and Co effect on nickel-ceria supported catalysts for ethanol steam reforming reaction. Int J Hydrogen Energy 2020;45:21512–22. https://doi.org/10.1016/J.IJHYDENE.2020.06.001.
[49] Megía PJ, Cortese M, Ruocco C, Vizcaíno AJ, Calles JA, Carrero A, et al. Catalytic behavior of co-based catalysts in the kinetic study of acetic acid steam reforming. Ind Eng Chem Res 2020;59:19531. https://doi.org/10.1021/acs.iecr.0c03599. –8.
[50] Li L, Song L, Wang H, Chen C, She Y, Zhan Y, et al. Water-gas shift reaction over CuO/CeO2 catalysts: effect of CeO2 supports previously prepared by precipitation with different precipitants. Int J Hydrogen Energy 2011;36:8839–49. https://doi.org/10.1016/J.IJHYDENE.2011.04.137.
[51] Isarapakdeetham S, Kim-Lohsoontorn P, Wongsakulphasatch S, Kiatkittipong W, Laosiripojana N, Gong J, et al. Hydrogen production via chemical looping steam reforming of ethanol by Ni-based oxygen carriers supported on CeO2 and La2O3 promoted Al2O3. Int J Hydrogen Energy 2020;45:1477–91. 10.1016/J.IJHYDENE.2019.11.077.
[52] Montero C, Ochoa A, Castaño P, Bilbao J, Gayubo AG. Monitoring Ni0 and coke evolution during the deactivation of a Ni/La2O3–αAl2O3 catalyst in ethanol steam reforming in a fluidized bed. J Catal 2015;331:181–92. https://doi.org/10.1016/j.jcat.2015.08.005.
[53] Kiani P, Meshksar M, Rahimpour MR. Biogas reforming over La-promoted Ni/SBA-16 catalyst for syngas production: catalytic structure and process activity investigation. Int J Hydrogen Energy 2023;48:6262–74. https://doi.org/10.1016/J.IJHYDENE.2022.02.232.

Please cite this article as: Megía PJ et al., Oxidative steam reforming of acetic acid on Ni catalysts: Influence of the La promotion on mesostructured supports, International Journal of Hydrogen Energy, https://doi.org/10.1016/j.ijhydene.2023.06.283